

# Journal of Mechanics of Materials and Structures

**NUMERICAL AND EXPERIMENTAL EVALUATION OF CRYOGENIC TENSILE  
STRENGTH OF WOVEN FABRIC-REINFORCED GLASS/EPOXY COMPOSITES  
USING OPEN HOLE SPECIMENS**

Yasuhide Shindo, Shinya Watanabe, Tomo Takeda, Fumio Narita, Takuya Matsuda  
and Satoru Yamaki

**Volume 6, No. 1-4**

**January–June 2011**

## NUMERICAL AND EXPERIMENTAL EVALUATION OF CRYOGENIC TENSILE STRENGTH OF WOVEN FABRIC-REINFORCED GLASS/EPOXY COMPOSITES USING OPEN HOLE SPECIMENS

YASUhide SHINDO, SHINYA WATANABE, TOMO TAKEDA,  
FUMIO NARITA, TAKUYA MATSUDA AND SATORU YAMAKI

A numerical and experimental evaluation of the tensile strength properties of woven glass fiber-reinforced polymer composite laminates at cryogenic temperatures was conducted by means of open hole specimens. Tensile tests were performed on specimens with a circular hole at room temperature, at 77 K, and at 4 K. The length of the hole edge damage zone corresponding to specimen failure was determined by microscopic examination of the fracture surfaces. A method based on finite element analysis was developed for estimating the cryogenic tensile strength of the unnotched woven laminates using the experimentally determined failure load and damage zone length. The results suggest that the tensile strength of woven composite laminates at cryogenic temperatures can be determined effectively by this approach.

### 1. Introduction

Fiber-reinforced polymer composites are widely used in many modern structural applications because of their unique properties. In particular, the demand for lightweight structures in the next generation of reusable launch vehicles may likely result in the use of carbon fiber-reinforced polymer (CFRP) composites in the design of the cryogenic liquid hydrogen and oxygen fuel tanks [Melcher and Johnson 2007]. Also, superconducting magnets for use in the International Thermonuclear Experimental Reactor (ITER) may use large quantities of woven glass fiber-reinforced polymer (GFRP) composite laminates as thermal and electrical insulation and structural support [Tsuji et al. 2001]. Hence, the mechanical properties of woven composite laminates must be characterized and fully understood under application-specific environmental conditions for the design process of cryogenic systems.

Accurate in-plane strength properties in tension of composite laminates are essential for material selection decision and as design data. Tensile tests have been a fundamental method of characterizing the mechanical response of composite materials for many years. The standard methods for tensile tests on composite materials — for example, American Society for Testing and Materials D 3039/D 3039M [ASTM 2000] and Japanese Industrial Standards K 7164 and K 7165 [JIS 2005; 2008] — are designed for room-temperature testing. However, there is currently no universally accepted method for tensile tests on composites at cryogenic temperatures. The determination of composite tensile properties, especially the ultimate strength, at cryogenic temperatures is not straightforward [Kumagai et al. 2003]. This is a result of the high strength, stiffness, and anisotropy of polymer matrix composite materials. Typically, cryogenic tensile tests on polymer matrix composites have resulted in noticeable inconsistencies with regard to strength values [Eisenreich and Cox 1992]. Also, cryogenic testing problems include that

*Keywords:* cryomechanics, finite element method, tension test, polymer-matrix composites, strength, cryogenic devices.

the specimen slips out of the test grips during testing. Increasing the clamping force to prevent grip slippage leads to increased stress concentration within the grip that influences the measured strength data. To address the problems encountered with cryogenic tensile testing, some researchers have devoted their efforts to evaluating the cryogenic mechanical response of composite specimens under tension. For example, Kumagai et al. [2004] experimentally and numerically examined the effects of specimen geometry and gripping method on the tensile properties of woven GFRP composite laminates having high glass content at cryogenic temperatures. Shindo et al. [2006] investigated the cryogenic mechanical response of woven GFRP composite specimens under tension, and discussed the influence of specimen geometry and size on the tensile properties of the composites.

An attractive alternative to the tensile test for the determination of the composite strength at cryogenic temperatures is the open hole tensile test. The open hole tensile test was originally developed to evaluate the notched strength (failure load divided by the gross cross-sectional area of composite laminates) [ASTM 2007]. However, the notched strength is not a material property but a structural property. For an open hole specimen, the failure load is correlated with the composite strength (a material property) and the size of the damage zone near the hole edge [Kogo et al. 1998; Green et al. 2007]. In addition, since the hole causes a stress concentration, the failure of the open hole specimen occurs at loads far below the failure load of the unnotched specimen. Therefore, the open hole tensile test offers a potentially attractive approach for avoiding cryogenic testing problems such as slippage between the specimen and the grips, and evaluating the composite strength.

A combined numerical-experimental method is presented for the evaluation of the tensile strength properties of woven GFRP composite laminates at cryogenic temperatures using open hole specimens. The open hole tensile tests were carried out at room temperature, liquid nitrogen temperature (77 K), and liquid helium temperature (4 K), and the failure loads were obtained. From microscopic examination of the fracture surfaces, the length of the damage zone at the hole edge was measured. The experimentally determined failure load and damage zone length were applied to the finite element model to estimate the cryogenic tensile strength of the unnotched woven laminates. The validity of this approach is discussed by comparing the predictions with existing experimental data.

## 2. Experimental procedure

**2.1. Material and specimen.** In this work, National Electrical Manufacturer's Association grade G-11 woven GFRP laminates (Arisawa Mfg. Co., Ltd., Japan) were used. The basis for G-11 woven laminates is a plain weave fabric of E-glass. The plain weave is produced by interlacing warp fiber bundles and fill fiber bundles. The weave contains 43 and 32 fiber bundles per 25.4 mm in the warp and fill directions, respectively. The polymer matrix is a bisphenol A epoxy resin. The overall fiber volume fraction is 47%.

Open hole specimens were employed for experiments. The geometry and dimensions of the specimen are shown in Figure 1. The specimens were cut with the length parallel to the warp direction. The dimensions of the specimen were 120 mm in overall length ( $l$ ), 27 mm in length of the grip section ( $g$ ), and 25 mm in width ( $w$ ). The nominal thickness of the specimen ( $h$ ) was equal to 2 mm. The specimens also contain a circular hole with a diameter ( $d$ ) of 4.2 mm in the center. The width to hole diameter ratio  $w/d$  was chosen based on the ASTM D 5766 standard [2007]. The tapered tabs were bonded to the sample ends by means of an adhesive system that is suitable for use at cryogenic temperatures.

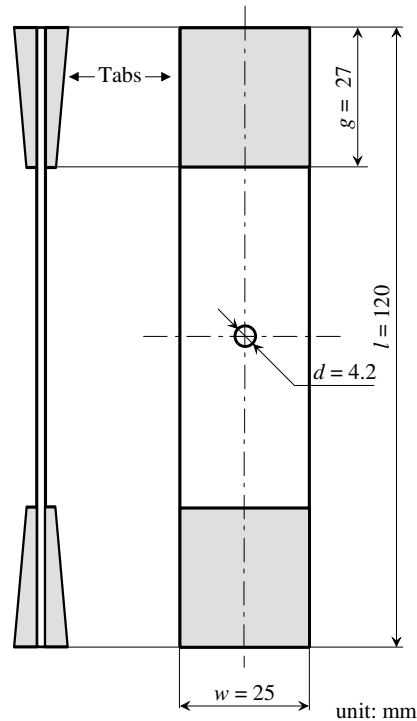


**Figure 1.** Geometry and dimensions of open hole specimen.

**2.2. Testing method.** Tensile tests were conducted on the open hole specimens at room temperature, 77 K, and 4 K using a 30 kN capacity servohydraulic testing machine. The strains were measured using strain gages bonded to the front and back surfaces of the specimen. The strain gages were placed near the hole as shown in Figure 2. Each specimen was tested at a displacement rate of 0.5 mm/min. Low-temperature environments were achieved by immersing the loading fixture and specimen in liquid nitrogen or liquid helium. To keep the specimen fully submerged in liquid helium during the test, an

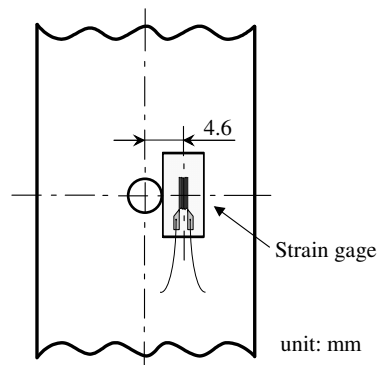


**Figure 2.** Position of the strain gage on open hole specimen.

automatic refill system (TRG-350D, Taiyo Nippon Sanso Co., Ltd., Japan) was incorporated. Load  $P$  and strain  $\varepsilon$  data were taken up to the catastrophic failure of the open hole specimens, and the failure loads  $P_c$  were measured.

Microscopic observations of the specimen surfaces and fracture surfaces were made with optical microscopy in order to obtain a better understanding of damage mechanisms of G-11 woven laminates at cryogenic temperatures. In addition, the fracture surfaces were examined in detail and the length of the critical damage zone (that is, the damage zone just before catastrophic failure),  $D_c$ , was determined from the fracture surface morphologies. All observations were performed after the completion of tensile testing.

### 3. Finite element analysis

Finite element simulations were carried out for the G-11 open hole specimens. The typical mesh of an open hole specimen is shown in Figure 3. The origin of the rectangular Cartesian coordinate system  $O$ - $xyz$  is fixed at the center of the open hole specimen, and the  $x$ ,  $y$ , and  $z$ -axes are in the fill, warp (tensile loading), and thickness directions, respectively. In the finite element calculations, plane stress conditions in the  $x$ - $y$  plane were assumed. The specimen was meshed using 6-noded triangular elements, and a relatively fine mesh was used adjacent to the hole in order to evaluate accurately the stress state.

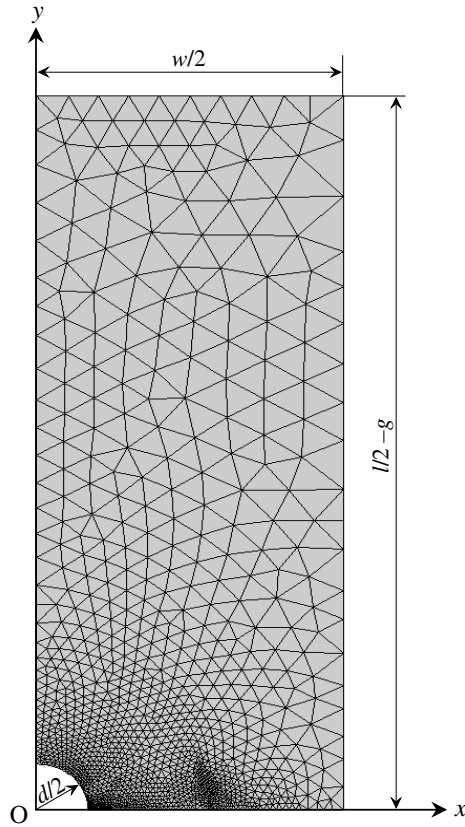


**Figure 3.** Finite element mesh of open hole specimen.

The finite element model treated the entire plain weave fabric composite as one homogeneous material with orthotropic material properties. Due to symmetry in geometry and loading, only one-quarter of the specimen was considered. The gripped portion was not included in the model.

The strain-stress relationships for the orthotropic composite specimen under plane stress are

$$\begin{bmatrix} \varepsilon_{xx}(x, y) \\ \varepsilon_{yy}(x, y) \\ 2\varepsilon_{xy}(x, y) \end{bmatrix} = \begin{bmatrix} 1/E_x & -\nu_{xy}/E_x & 0 \\ -\nu_{xy}/E_x & 1/E_y & 0 \\ 0 & 0 & 1/G_{xy} \end{bmatrix} \begin{bmatrix} \sigma_{xx}(x, y) \\ \sigma_{yy}(x, y) \\ \sigma_{xy}(x, y) \end{bmatrix}, \quad (1)$$

where  $\varepsilon_{xx}(x, y)$ ,  $\varepsilon_{yy}(x, y)$ , and  $\varepsilon_{xy}(x, y) = \varepsilon_{yx}(x, y)$  are the strain components;  $\sigma_{xx}(x, y)$ ,  $\sigma_{yy}(x, y)$ , and  $\sigma_{xy}(x, y) = \sigma_{yx}(x, y)$  are the stress components;  $E_x$  and  $E_y$  are the Young's moduli;  $G_{xy}$  is the shear modulus; and  $\nu_{xy} = \nu_{yx}E_x/E_y$  is the Poisson's ratio. The Poisson's ratio  $\nu_{xy}$  reflects shrinkage (expansion) in the  $y$ -direction, due to tensile (compressive) stress in the  $x$ -direction. The normal strain component  $\varepsilon_{zz}$  perpendicular to the  $x$ - $y$  plane can be expressed in terms of the stress components  $\sigma_{xx}(x, y)$  and  $\sigma_{yy}(x, y)$  and the elastic properties  $E_x$ ,  $E_y$ ,  $\nu_{xz} = \nu_{zx}E_x/E_z$ , and  $\nu_{yz} = \nu_{zy}E_y/E_z$  as follows:

$$\varepsilon_{zz}(x, y) = -\frac{\nu_{xz}}{E_x}\sigma_{xx}(x, y) - \frac{\nu_{yz}}{E_y}\sigma_{yy}(x, y). \quad (2)$$

The elastic properties  $E_x$ ,  $E_y$ ,  $E_z$ ,  $G_{xy}$ ,  $\nu_{xy}$ ,  $\nu_{yz}$ , and  $\nu_{zx}$  were determined from the micromechanics model for plain weave fabric composites [Hahn and Pandey 1994]. The model includes parameters to characterize the fabric architecture and constituent material properties. The geometrical parameters of G-11 woven laminates were measured on scanning electron microscopy photographs of the woven laminate cross-sections. The Young's modulus, shear modulus, and Poisson's ratio of the matrix and fiber were obtained from the exponential functions of temperature based on the experimental data [Dahlerup-Petersen and Perrot 1979]. The composite elastic moduli can be determined under the assumption of uniform strain inside the unit cell. Table 1 lists the predicted Young's moduli  $E_x$ ,  $E_y$ , and  $E_z$ , shear modulus  $G_{xy}$ , and Poisson's ratios  $\nu_{xy}$ ,  $\nu_{yz}$ , and  $\nu_{zx}$  of G-11 woven laminates at 295 K (room temperature), 77 K, and 4 K. In the table, the values in parentheses are the experimental results [Sanada and Shindo 2005]. By comparing the predicted elastic moduli with experimental data, this model is shown to be efficient and accurate.

In [Whitney and Nuismer 1974] two stress failure criteria were proposed, the point stress criterion (PSC) and the average stress criterion (ASC), for predicting the point at which the catastrophic failure of

	295 K	77 K	4 K
$E_x$ (GPa)	21.07 (24.1)	28.47 (31.1)	31.95 (34.3)
$E_y$ (GPa)	26.66 (27.9)	32.98 (32.7)	35.94 (36.9)
$E_z$ (GPa)	10.75	20.48	25.03
$G_{xy}$ (GPa)	5.17 (6.2)	8.76 (9.4)	10.28 (10.1)
$\nu_{xy}$	0.10	0.16	0.19
$\nu_{yz}$	0.32	0.33	0.34
$\nu_{zx}$	0.17	0.26	0.29

**Table 1.** Predicted elastic moduli of G-11 woven laminates.

a laminated composite with a circular hole occurs. These two stress criteria use the linear elastic stress field adjacent to the hole, and are semiempirical models based on the laminate tensile strength and a characteristic dimension. The characteristic dimension seems to be related to the length of the damage zone at the hole edge [Kogo et al. 1998]. With regard to the above criteria, Belmonte et al. [2001] have pointed out that the ASC is more consistent with the experimental results on damage growth and failure at circular holes in woven GFRP composite laminates under tension at room temperature than the PSC. While the ASC has the merits of being simple to apply, its limitations are that it does not consider the evolution of damage from the hole. In practice the damage will modify, significantly, the assumed elastic stress distribution near the hole, and the ASC does not give an adequate description of the stress state. Actually, the stress distribution in the damage zone is very complicated. Although the stress level along the direction perpendicular to the applied tensile load inside the damage zone can be considered to keep nearly constant and the stress is correlated with the unnotched tensile strength [Zhen 1983], no one has evaluated exactly the stress state near the hole in the damaged composites. In the present study, the damage zone was therefore modeled as a strip with the critical damage zone length  $D_c$  ahead of the hole edge, and the normal stress  $\sigma_{yy}$  was assumed to be uniform within the damage zone. Let  $u_x$  and  $u_y$  be the displacement components. The boundary conditions can be written as

$$\sigma_{yy}(x, 0) = \sigma_0 \quad \text{for} \quad d/2 \leq x < d/2 + D_c, \quad (3)$$

$$u_y(x, 0) = 0 \quad \text{for} \quad d/2 + D_c \leq x \leq w/2, \quad (4)$$

$$\sigma_{yx}(x, 0) = 0 \quad \text{for} \quad d/2 \leq x \leq w/2, \quad (5)$$

$$u_y(x, l/2 - g) = u_y^* \quad \text{for} \quad 0 \leq x \leq w/2, \quad (6)$$

$$\sigma_{yx}(x, l/2 - g) = 0 \quad \text{for} \quad 0 \leq x < w/2, \quad (7)$$

$$u_x(0, y) = 0 \quad \text{for} \quad d/2 \leq y \leq l/2 - g, \quad (8)$$

$$\sigma_{xy}(0, y) = 0 \quad \text{for} \quad d/2 \leq y \leq l/2 - g, \quad (9)$$

$$\sigma_{xx}(w/2, y) = 0 \quad \text{for} \quad 0 \leq y < l/2 - g, \quad (10)$$

$$u_x(w/2, l/2 - g) = 0 \quad (11)$$

$$\sigma_{xy}(w/2, y) = 0 \quad \text{for} \quad 0 \leq y < l/2 - g, \quad (12)$$

where  $\sigma_0$  is the uniform stress in the damage zone and  $u_y^*$  is the prescribed displacement in the  $y$ -direction. The prescribed displacement  $u_y^*$  was determined from the condition

$$\frac{2}{w} \int_0^{w/2} \sigma_{yy}(x, l/2 - g) dx = \frac{P_c}{wh}. \quad (13)$$

The displacement boundary condition given in (11) represents the constraint effect resulting from the rigid clamping of the specimen's ends. The stress distribution corresponding to the experimentally obtained failure load  $P_c$  and critical damage zone length  $D_c$  was determined from the finite element analysis, as illustrated in Figure 4. The solid and dashed lines in the figure represent the stress distributions near the hole with and without the damage zone, respectively. The solid line can be obtained using the condition of finite stress  $\sigma_0$  (vanishing stress singularity) at the tip  $x = d/2 + D_c$ , and the  $\sigma_0$  value was evaluated

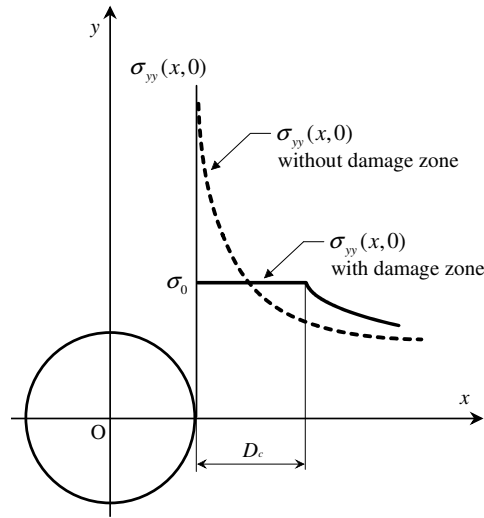


**Figure 4.** Stress distribution near the hole with damage zone.

for each specimen. The numerically evaluated uniform stress  $\sigma_0$  was regarded as the ultimate tensile strength of the specimen material.

**4. Results and discussion**

Figure 5 shows the measured gage strains  $\epsilon$  in percent as a function of the applied stress  $\sigma$  ( $\sigma = P/wh$ ) at room temperature (RT), 77 K, and 4 K. For the sake of comparison, a linear elastic finite element analysis was carried out and the calculated strains are also provided in the figure (the dashed lines). The calculated strain is the normal strain in the y-direction at the center of the strain gage ( $x = 4.6, y = 0$ )

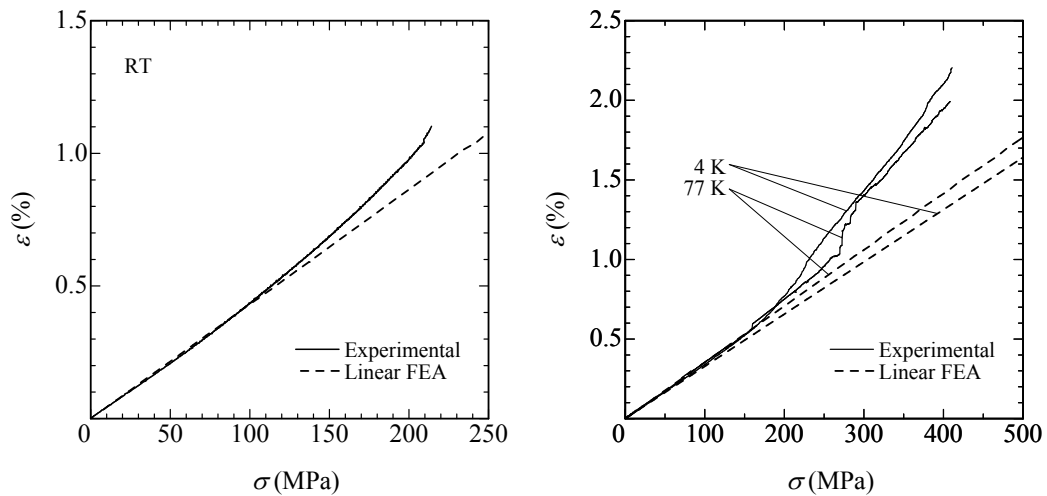


**Figure 5.** Measured and calculated gage strains versus applied stress at room temperature (left) and at 77 K and 4 K (right).

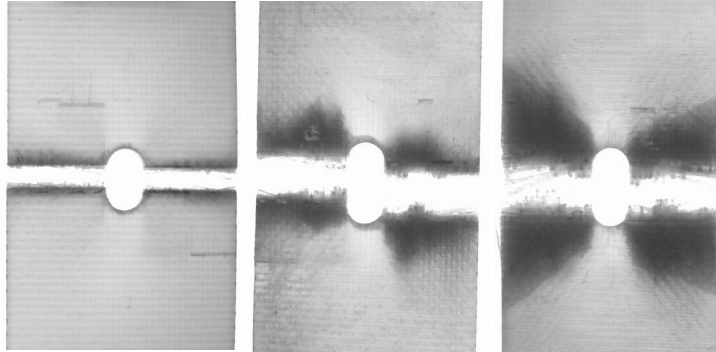


**Figure 6.** Photographs of failed specimens at room temperature (left), 77 K (middle), and 4 K (right).

and corresponds to the measured gage strain. The linear analysis did not consider the hole edge damage ( $D_c = 0$ ). Each curve exhibits a linear initial region, and the calculated curves agree with the experimental data very well. With increase in the applied stress, the nonlinearity of the curves appears at both room temperature and cryogenic temperatures. Note that pronounced nonlinearity of the curves can be found at 77 K and 4 K, which can be attributed to the accumulation of damage such as microcracks in the matrix material [Takeda et al. 2005].

Photographs of the open hole specimens after the tensile tests at room temperature, 77 K, and 4 K are shown in Figure 6. Failure invariably occurs in the central section of the specimens. A straight failure plane is formed normal to the applied load at room temperature. In the specimens at 77 K and 4 K, an intense damage zone is found at the hole edge. Also, the size of the damage in the specimen at 4 K is more extensive than that at 77 K. This damage zone is generally seen on both sides of the hole. Figure 7 shows the optical microscopy images of the edge sections of failed specimens at room temperature, 77 K, and 4 K. It can be seen that the specimen at 4 K shows extensive delamination, while the specimen at 77 K displays less delamination, and the specimen at room temperature virtually none. This may be

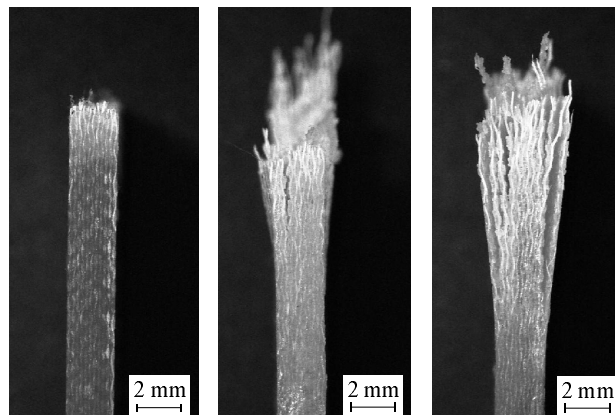


**Figure 7.** Edge views of failed specimens at room temperature (left), 77 K (middle), and 4 K (right).

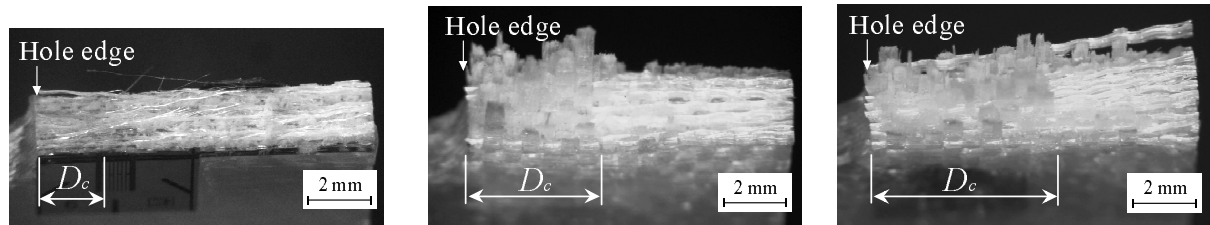


**Figure 8.** Fracture surface morphologies of failed specimens at room temperature (left), 77 K (middle), and 4 K (right).

due to the residual thermal stresses in the specimens generated during cooling and the brittleness of the polymer resins at cryogenic temperatures. Figure 8 shows typical fracture surface morphologies of failed specimens at room temperature, 77 K, and 4 K. The fracture surface displays the drastic difference in failure mechanism between room temperature and cryogenic temperatures. The region of the room temperature fracture surface near the hole edge is relatively smooth, and loose transverse (fill) fiber bundles are found away from the hole edge. Loose transverse fiber bundles are a characteristic of woven laminate tensile failure at room temperature [Karayaka and Kurath 1994]. Based on this finding, damage before the catastrophic failure of the open hole specimens at room temperature seems to lead to the smooth fracture surface near the hole edge and the length of the smooth region is taken as the critical damage zone length  $D_c$  at room temperature. At 77 K and 4 K, the fracture surfaces near the hole edge exhibit fiber pullout, and the fibers tend to pull out as bundles rather than individual filaments. Damage (microcracks) caused by large residual thermal stresses at cryogenic temperatures and concentrated stresses near the hole lead to the degradation in the fiber-matrix interface bonding and the fiber breakage. In the case of poor fiber-matrix bonding, the broken fibers are pulled out of the matrix [Berthelot 1999]. The fracture surfaces at 77 K and 4 K suggest that the length of the fiber pullout region corresponds to the critical damage zone length  $D_c$ . Overall the fracture surface studies indicate that the smooth region at room temperature and the fiber pullout region at 77 K and 4 K were localized near the hole edge, and the boundary of the damage zone was discerned relatively well. Table 2 shows the experimentally obtained failure loads  $P_c$  and critical damage zone lengths  $D_c$  at room temperature, 77 K, and 4 K. The critical damage zone length  $D_c$  in the table was calculated as the average of the values measured on both sides of the hole after the tensile test of each specimen. The failure loads at 77 K and 4 K are higher than that at room temperature, and the failure load at 77 K is similar to that at 4 K. The critical damage zone length increases as the temperature decreases. The difference in the critical damage zone length reflects the microdamage mechanism changes with changing temperature. Also, the critical damage zone length

RT		77 K		4 K	
$P_c$ (kN)	$D_c$ (mm)	$P_c$ (kN)	$D_c$ (mm)	$P_c$ (kN)	$D_c$ (mm)
10.8	1.9	20.4	5.7	20.8	6.8
10.7	2.0	21.7	4.9	22.3	6.8
10.5	2.6	21.2	5.2	20.7	6.7

**Table 2.** Failure loads  $P_c$  and critical damage zone lengths  $D_c$ .

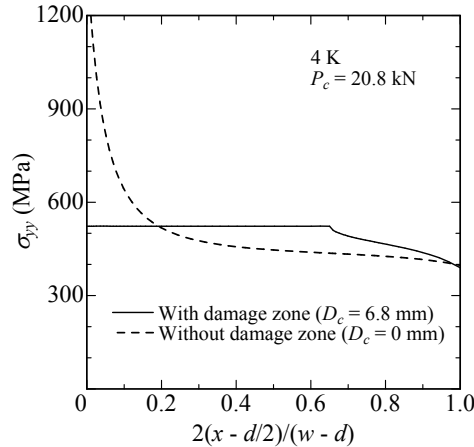


**Figure 9.** Stress distributions near the hole along the line  $y = 0$  ( $d/2 \leq x \leq w/2$ ).

at each temperature is reasonably constant across all specimens. This implies that the measurement of the critical damage zone length is reliable.

Figure 9 shows the distributions of the normal stresses  $\sigma_{yy}$  along the  $x$ -axis ( $y = 0$ ,  $d/2 \leq x \leq w/2$ ) with and without the damage zone at 4 K as a function of distance from the hole edge  $2(x - d/2)/(w - d)$ . The failure load  $P_c$  and the critical damage zone length  $D_c$  were taken as 20.8 kN and 6.8 mm, respectively. Based on the stress distribution with the damage zone, the uniform stress  $\sigma_0$  in the damage zone can be determined to be 523 MPa. Table 3 presents the numerically determined uniform stresses  $\sigma_0$  at room temperature, 77 K, and 4 K. The uniform stresses  $\sigma_0$  in the table are averages of three values at each temperature, and the values in parentheses are the standard deviations. For comparison, the ultimate tensile strengths  $\sigma_{ult}$  from the tensile tests on the unnotched G-11 specimens [Shindo et al. 2006] are given in the table. The numerically determined uniform stresses  $\sigma_0$  are in good agreement with the  $\sigma_{ult}$  values. This suggests that the uniform stress from the present combined numerical-experimental method is a reliable estimate of the composite tensile strength at cryogenic temperatures. It may be possible to carry out the cryogenic tensile tests on the unnotched specimens of the commercial G-11 woven laminates. However, cryogenic tensile testing is very difficult for high-strength advanced composite materials such as CFRP composites. Although the issue of grip slippage in unnotched tests, of course, has to be overcome, the present method is an efficient approach to measuring the cryogenic tensile strength of high-strength composite materials because high applied tensile load and high clamping force are not necessary to break the open hole specimen.

RT		77 K		4 K	
$\sigma_0$ (MPa)	$\sigma_{ult}$ (MPa)	$\sigma_0$ (MPa)	$\sigma_{ult}$ (MPa)	$\sigma_0$ (MPa)	$\sigma_{ult}$ (MPa)
331	310	548	610	535	579
(13.9)	(28.7)	(18.8)	(73.1)	(18.4)	(14.0)

**Table 3.** Predicted and experimental ultimate tensile strengths of G-11 woven composite laminates. Values in parentheses are standard deviations in a sample of size three.

## 5. Conclusions

In this article, we studied the tensile strength properties of woven glass fiber-reinforced polymer composite laminates at cryogenic temperatures through a combined numerical-experimental approach using open hole specimens. The major conclusion from the current investigation is that it is possible to obtain reasonable values of the ultimate tensile strength of woven laminates at cryogenic temperatures from open hole specimens. Also, at cryogenic temperatures, microscopic examination of the failed specimens suggests that an intense damage zone develops at the hole edge prior to catastrophic failure. The open hole acts as sufficient stress riser to force the specimen failure from the hole, and, therefore, the present method provides a novel approach to measuring the cryogenic tensile strength of high-strength advanced composite materials.

## Dedication

We dedicate this work to the memory of Marie-Louise. As Associate Editor of the *International Journal of Solids and Structures* and the *Journal of Mechanics of Materials and Structures*, she devoted herself to the success of those journals, and we owe her much for their progress. When I first met her and Charles for the first time in 1994, in Seattle, she talked to me as a friend. Since then, I enjoyed various discussions with them at conferences. I miss her. We thank Marie-Louise and Charles Steele for their efforts and dedication to two successful journals.

## References

- [ASTM 2000] “Standard test method for tensile properties of polymer matrix composite materials”, Standard ASTM D3039/D3039M-00<sup>ε1</sup>, American Society for Testing and Materials, Philadelphia, 2000. Superseded by the active standard.
- [ASTM 2007] “Standard test method for open hole tensile strength of polymer matrix composite laminates”, Standard ASTM D5766/D5766M-02a, American Society for Testing and Materials, Philadelphia, 2007. reapproved 2007. Superseded by the active standard.
- [Belmonte et al. 2001] H. M. S. Belmonte, C. I. C. Manger, S. L. Ogin, P. A. Smith, and R. Lewin, “Characterisation and modelling of the notched tensile fracture of woven quasi-isotropic GFRP laminates”, *Compos. Sci. Technol.* **61**:4 (2001), 585–597.
- [Berthelot 1999] J.-M. Berthelot, *Composite materials: mechanical behavior and structural analysis*, Springer, New York, 1999.
- [Dahlerup-Petersen and Perrot 1979] K. Dahlerup-Petersen and A. Perrot, “Properties of organic composite materials at cryogenic temperatures”, Technical report CERN-ISR-BOM-79-39, European Organization for Nuclear Research (CERN), Geneva, November 1979, available at <http://cdsweb.cern.ch/record/312298>.
- [Eisenreich and Cox 1992] T. J. Eisenreich and D. S. Cox, “Modification of the ASTM D 3039 tensile specimen for cryogenic applications”, *Adv. Cryog. Eng.* **38** (1992), 437–444.
- [Green et al. 2007] B. G. Green, M. R. Wisnom, and S. R. Hallett, “An experimental investigation into the tensile strength scaling of notched composites”, *Compos. A Appl. Sci. Manuf.* **38**:3 (2007), 867–878.
- [Hahn and Pandey 1994] H. T. Hahn and R. Pandey, “A micromechanics model for thermoelastic properties of plain weave fabric composites”, *J. Eng. Mater. Technol. (ASME)* **116**:4 (1994), 517–523.
- [JIS 2005] “Plastics – Determination of tensile properties – Part 4: Test conditions for isotropic and orthotropic fibre-reinforced plastic composites”, Standard JIS K 7164:2005, Japanese Standards Association, Tokyo, 2005.
- [JIS 2008] “Plastics – Determination of tensile properties – Part 5: Test conditions for unidirectional fibre-reinforced plastic composites”, Standard JIS K 7165:2008, Japanese Standards Association, Tokyo, 2008.

- [Karayaka and Kurath 1994] M. Karayaka and P. Kurath, "Deformation and failure behavior of woven composite laminates", *J. Eng. Mater. Technol. (ASME)* **116**:2 (1994), 222–232.
- [Kogo et al. 1998] Y. Kogo, H. Hatta, H. Kawada, and T. Machida, "Effect of stress concentration on tensile fracture behavior of carbon-carbon composites", *J. Compos. Mater.* **32**:13 (1998), 1273–1294.
- [Kumagai et al. 2003] S. Kumagai, Y. Shindo, K. Horiguchi, and T. Takeda, "Mechanical characterization of CFRP woven laminates between room temperature and 4K", *JSME Int. J. Series A* **46**:3 (2003), 359–364.
- [Kumagai et al. 2004] S. Kumagai, Y. Shindo, K. Horiguchi, and F. Narita, "Experimental and finite-element analysis of woven glass-cloth/epoxy laminate tensile specimen at room and low temperatures", *Mech. Adv. Mater. Struct.* **11**:1 (2004), 51–66.
- [Melcher and Johnson 2007] R. J. Melcher and W. S. Johnson, "Mode I fracture toughness of an adhesively bonded composite-composite joint in a cryogenic environment", *Compos. Sci. Technol.* **67**:3–4 (2007), 501–506.
- [Sanada and Shindo 2005] K. Sanada and Y. Shindo, "Cryogenic damage and fracture behaviors of G-11 woven glass-epoxy laminates", *JSME Int. J. Series A* **48**:2 (2005), 91–99.
- [Shindo et al. 2006] Y. Shindo, F. Narita, K. Horiguchi, S. Takano, T. Takeda, and K. Sanada, "Tensile behavior and damage/acoustic emission characteristics of woven glass fiber reinforced/epoxy composite laminates at cryogenic temperatures", *Adv. Cryog. Eng.* **52** (2006), 249–256.
- [Takeda et al. 2005] T. Takeda, S. Takano, Y. Shindo, and F. Narita, "Deformation and progressive failure behavior of woven-fabric-reinforced glass/epoxy composite laminates under tensile loading at cryogenic temperatures", *Compos. Sci. Technol.* **65**:11–12 (2005), 1691–1702.
- [Tsuji et al. 2001] H. Tsuji, S. Egorov, J. Minervini, M. Martovetsky, K. Okuno, Y. Takahashi, and R. J. Thome, "ITER R&D: magnets: central solenoid model coil", *Fusion Eng. Des.* **55**:2–3 (2001), 153–170.
- [Whitney and Nuismer 1974] J. M. Whitney and R. J. Nuismer, "Stress fracture criteria for laminated composites containing stress concentrations", *J. Compos. Mater.* **8**:3 (1974), 253–265.
- [Zhen 1983] S. Zhen, "The D criterion theory in notched composite materials", *J. Reinf. Plast. Compos.* **2**:2 (1983), 98–110.

Received 31 Mar 2010. Revised 11 Oct 2010. Accepted 13 Oct 2010.

YASUhide SHINDO: shindo@material.tohoku.ac.jp

Tohoku University, Department of Materials Processing, Graduate School of Engineering, Aoba-ku, Sendai 980-8579, Japan

SHINYA WATANABE: Tohoku University, Department of Materials Processing, Graduate School of Engineering, Aoba-ku, Sendai 980-8579, Japan

TOMO TAKEDA: takeda-t@material.tohoku.ac.jp

Tohoku University, Department of Materials Processing, Graduate School of Engineering, Aoba-ku, Sendai 980-8579, Japan

FUMIO NARITA: narita@material.tohoku.ac.jp

Tohoku University, Department of Materials Processing, Graduate School of Engineering, Aoba-ku, Sendai 980-8579, Japan

TAKUYA MATSUDA: Tohoku University, Department of Materials Processing, Graduate School of Engineering, Aoba-ku, Sendai 980-8579, Japan

SATORU YAMAKI: Tohoku University, Department of Materials Processing, Graduate School of Engineering, Aoba-ku, Sendai 980-8579, Japan